Preliminary Analysis of RFI Signals Captured using the CISR Coherent Sampling Mode

Steven W. Ellingson*

March 4, 2005

Contents

*Bradley Dept. of Electrical & Computer Engineering, 340 Whittemore Hall, Virginia Polytechnic Institute & State University, Blacksburg VA 24061 USA. E-mail: ellingson@vt.edu

1 Introduction

This report summarizes a study of radio frequency interference (RFI) in the CISR "capture" data sets from recent airborne experiments. In these experiments, the CISR digital backend was integrated with NOAA's "PSR/C" system in a co-observing configuration [1]. PSR/C itself is strictly a total power (incoherent) sampling radiometer, with time-frequency resolution limited to milliseconds and 100's of MHz, respectively. The severe RFI environment in C-band significantly degrades the quality of radiometry obtained by PSR/C and other instruments. At the same time, the limited time-frequency resolution of these instruments provides only limited information as to the nature of the RFI. In these experiments, the CISR backend is used in parallel with the PSR/C backend to provide greatly enhanced time-frequency resolution, offering improved ability to identify and characterize RFI. The results may be used to devise RFI mitigation algorithms which could be incorporated into CISR and future C-band radiometers.

2 Methodology

2.1 Hardware Configuration and Data Capture

The PSR/C front end uses conical scanning antenna which completes an azimuthal cycle every 3 s. Simultaneously, the front end sweeps from 5.5 GHz to 7.7 GHz ("C-band", for the purposes of this discussion) in 22 steps, completing ~ 3.6 sweeps per azimuthal cycle. This signal is downconverted to a 125 MHz intermediate frequency (IF) using a single-sideband ("image rejection") mixer, which also determines the current center frequency. One limitation of this architecture is that the mixer is known to have image rejection of only about 18 dB. Thus, signals observed by CISR at any given frequency may actually be at a frequency 250 MHz away and ~ 18 dB greater. The observed density of RFI in the data sets appears to be sufficiently low that this does not spoil the usefulness of the data; however, since some of the data (including RFI) exhibits dynamic range in excess of 20 dB, the potential for cross-talk from the image band should be kept in mind.

The 125 MHz IF is split into two 50 MHz segments: 75–125 MHz and 125–175 MHz. The latter is directly digitized by one of CISR's 10-bit 200 MSPS digitizers. The former is frequency-shifted to 125–175 MHz and digitized in the same manner by CISR's other digitizer. The two half-bands are downconverted, filtered, resampled, and combined into a single 100 MSPS complex-valued signal, encoding ~ 80 MHz contiguous bandwidth. This output is captured in blocks of 128K (128×1024) contiguous samples, yielding a data record ~ 1.3 ms in length. The blocks however are not contiguous; the minimum time between blocks is at least 38 ms, although this separation is often much greater as CISR periodically cycles through other modes of operation, during which time coherent data is not captured.

Although the means exist to do so, no attempt has been made to associate any of the 128K sample blocks analyzed here with the C-band frequency or antenna pointing at the time of capture.

This report addresses two distinct data sets. The first is that from the directory "set of 182 12.20 to 14.00", known henceforth as "file set 182"; and the second is that from the directory "set of 391 16.40 on", known henceforth as "file set 391".

2.2 Data Analysis

Data analysis was conducted in two phases. In the first phase, both file sets were processed using a survey program, described below, which searched each block for RFI events. The results of this survey were compiled and are reported in Figure 4. In the second phase, a few blocks of data were searched manually, in order to better understand the time-frequency characteristics of the various RFI encountered. The results of this phase of analysis are reported in Sections 3.2 and 3.3.

The survey program works as follows: First, the 128K samples are partitioned into 1K sets of 128 samples each. Each of these sets is FFTed (without windowing) to obtain a power spectrum. The frequency response of the instrument is then removed from these spectra by *baseline correction*. Baseline correction involves normalizing the mean power spectral density (PSD) to unity and then dividing bin-by-bin by a precomputed "baseline spectrum" which is normalized to unit-mean power spectral density. The baseline spectrum used here is shown in Figure 1, and was computed using a combination of mean normalization and integration over several blocks which appeared to be RFI-free. The 1K baseline-corrected spectra are then assembled into a 128×1024-pixel "spectrogram" consisting of 128K pixels having time-frequency dimensions of 781.25 kHz and 1.28 μs, respectively.

An example of the result at this stage of the analysis is shown in Figure 2, which shows a block containing no obvious RFI. In this report, two auxiliary plots are provided with each spectrogram: One showing PSD averaged over time (i.e., a "vertical averaging" of the spectrogram) and another showing total power averaged over frequency (i.e., a "horizontal averaging" of the spectrogram). The auxiliary plots sometimes reveal RFI not apparent in the spectrogram, and vice versa. Note that since the received noise is nominally Gaussian and the mean PSD is now unity, the units of PSD in the spectrogram are standard deviations (σ) with respect to the noise distribution.

Figure 3 shows the statistics of PSD for the spectrogram shown in Figure 2, which is essentially the same result obtained for any block with no obvious RFI. Note that many pixels exhibit significant deviation from the expected Gaussian trend line beginning at about 5σ. Many pixels with PSDs greater than 10σ are quite far removed from the Gaussian noise trend line and thus are almost certainly RFI of some sort. In this report, we adopt a very high threshold of 19σ for detection of RFI on a pixel-by-pixel basis. The justification for this is that it has been observed by experimentation that the impact of RFI-contaminated pixels below this level are very unlikely to significantly bias total power measurements for remote sensing.

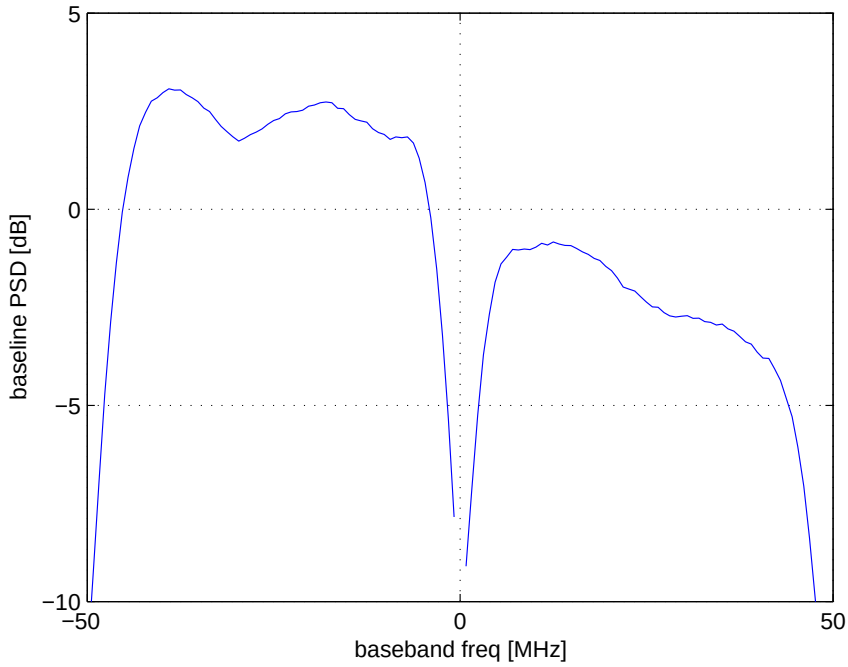

Figure 1: Baseline spectrum used for baseline correction. The null in the center is due to the "stitching together" of two separate subbands in the CISR receiver to form a single signal. The reason for the reduced gain and uneven slope of the upper subband is not known, but probably arises in the splitting and recentering of the 125 MHz analog IF.

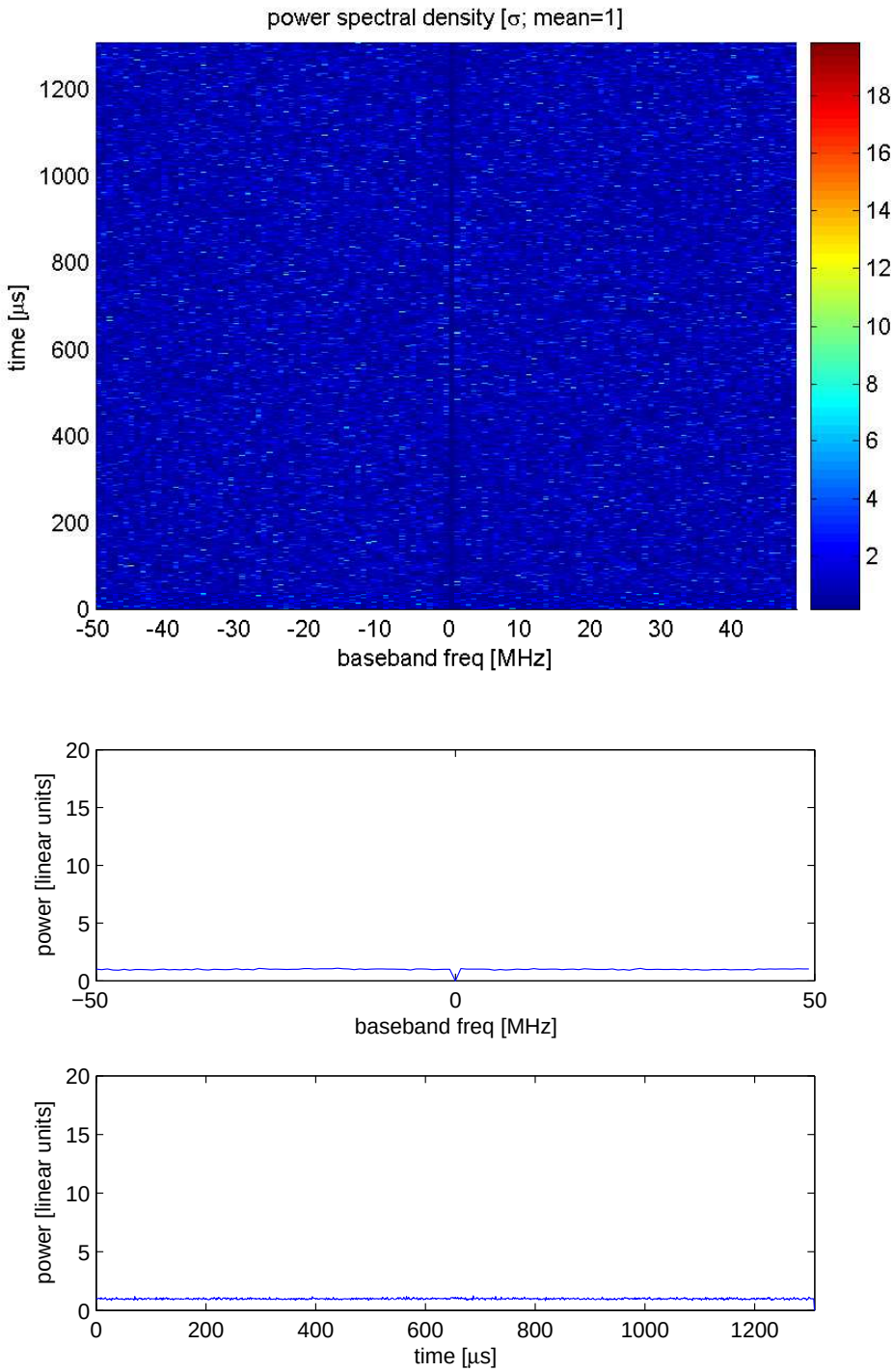

Figure 2: A typical spectrogram and auxiliary plots for a block with no obvious RFI.

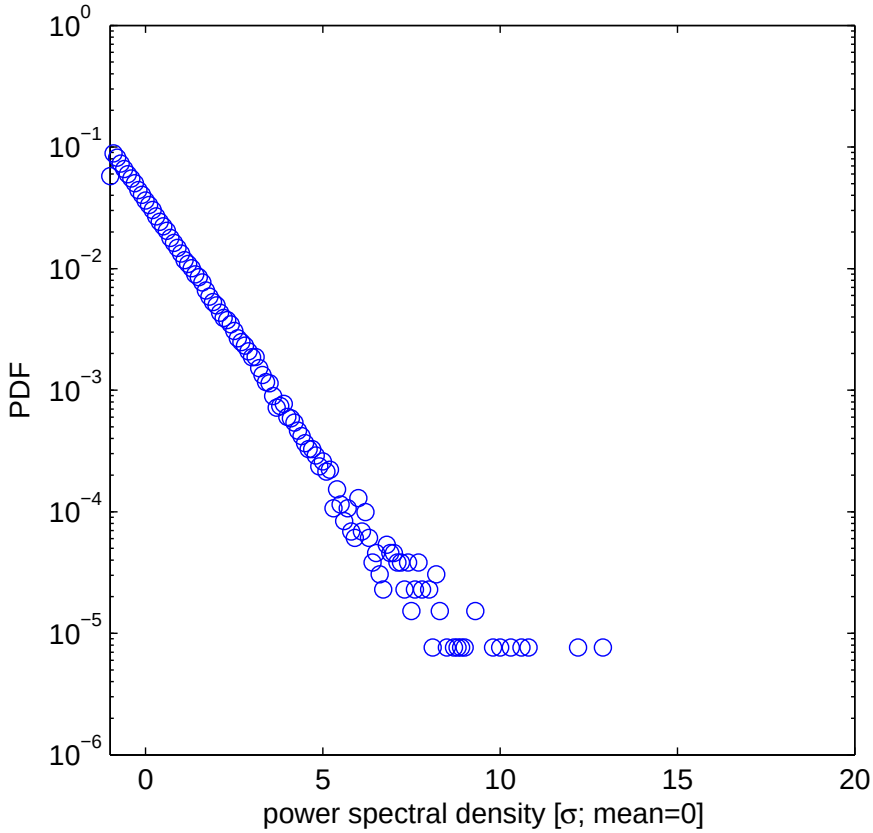

Figure 3: Histogram of pixel PSD for Figure 2. (Note that in this plot only, the mean was arbitrarily shifted from 1 to zero.)

In addition to "pixel" events, the survey program also searches for "bin" events. A bin event is declared for any bin in a spectrogram which has an average PSD greater than 0.4σ above the mean. Bin detection provides increased sensitivity for persistent, narrowband interference which may be too weak to detect on a pixel-by-pixel basis. The effectiveness of this detector is another reason for setting the pixel detection threshold relatively high, so as to limit the possibility of detecting persistent band-limited RFI as both a single bin event and many pixel events.

Finally, it should be noted that the process of baseline correction also removes variations in total power over time scales greater than 1.28 μs. If the instrument is external-noise dominated, this causes the magnitude of the received RFI signals to be biased in inverse proportion to the total power of the noise. So, for example, the actual power of an RFI signal will be biased downward while PSR is observing land, relative to the same signal power received while PSR is observing ocean, which normally has a lower brightness temperature. However, this variation is over a range of about 4:1 (6 dB) at most, and so is probably is not much of an issue in this study compared to other factors. In any event, the signal-to-noise ratio is preserved, so there is no effect on sensitivity.

3 Results

3.1 Statistics

Figure 4 provides a summary of the findings using the survey program applied to file sets 391 and 182. It is noted that file set 391 exhibits about twice as many RFI event detections per unit time as file set 182, but otherwise the file sets appear similar. Perhaps the key finding is that about 7% of blocks (3% for file set 182) examined were found to contain some form of RFI. The "bottom line" question though is to what extent this RFI degrades total power radiometry. As shown in Figure 4, it is found that persistent band-limited RFI (as detected via bin events) seems to be a prevalent source of contamination to total power radiometry in the observed frequencies, with more than 5% of the blocks analyzed having total power which was biased at by least 5% by this form of RFI. Single pixel RFI was similarly damaging in that only about 0.2% of blocks (0.004% from file set 182) were likewise biased. Figure 5 shows PDFs of the magnitudes of all bin and pixel detections for both file sets.

3.2 Pulse Detections

One of the dominant sources of RFI at L-band are radar pulses, so close attention was paid to this possibility of this being true at C-band as well. The radar pulses seen at L-band are typically between 2 μs and 400 μs in duration, with bandwidths between a few hundred kHz and tens of MHz and repetition periods on the order of milliseconds. Thus, the survey program is most likely to identify them through pixel detections. Although Figure 4 reveals that pixel detections account for only a small percentage of the significant RFI, a few signals which are probably radars were

File Set	"391"	"182"	Remarks
Total Files	288	86	
Total Blocks	12,672	3784	44 blocks/file (1.31 ms/block)
Total Bins	1.622×10^6	4.843×10^5	128 bins/block (781.25 kHz/bin)
Total Pixels	1.661×10^9	4.960×10^8	128×1024 pixels/block
			(781.25 kHz $\times$ 1.28 μs / pixel)
Bins w/RFI	4275 (0.264%)	564 (0.1165%)	mean noise $+0.4\sigma$ threshold
Pixels w/RFI	32,561 (0.002%)	2037 (0.0004%)	mean noise $+19\sigma$ threshold
Blocks w/RFI	888 (7.008%)	109 (2.8805%)	Containing detections of either kind
Due to bins:			
Blocks w/RFI bias $\geq 5\%$	668 (5.271%)	88 (2.3256%)	
Blocks w/RFI bias $\geq 1\%$	668 (5.271%)	88 (2.3256%)	
Blocks w/RFI bias $\geq 0.2\%$	668 (5.271%)	88 (2.3256%)	
Due to pixels:			
Blocks w/RFI bias $\geq 5\%$	26 (0.205%)	2 (0.0528%)	
Blocks w/RFI bias $\geq 1\%$	73 (0.576%)	8 (0.2114%)	
Blocks w/RFI bias $\geq 0.2\%$	123 (0.971%)	14 (0.3700%)	

Figure 4: Summary of the findings of this study.

detected. The best candidate is shown in Figure 6, with follow up analysis shown in 7. Figure 7(a) and (c) indicate a pulse length of $\sim$ 2μs. Figure 7(b) indicates that this is a dual-frequency pulse, with the detected component appearing at a baseband frequency of about -40 MHz and an a weaker, undetected component appearing at about $+40$ MHz. Figure 7(d) shows the stronger pulse to have a bandwidth of about 1 MHz. Each of the two component pulses are almost certainly CW-modulated; this is confirmed in Figure 7(c) by noting that the large time-domain magnitude variation (which would normally suggest some kind of digital modulation) is almost completely removed when one of the two pulses is filtered out. The time-frequency characteristics of this pulse are consistent with characteristics of similar pulses routinely observed at L-band, including the use of two pulses separated in frequency [2].

File 27 of file set 391 shows several examples of probable radar pulses. One example is shown in Figure 8, with follow up in Figure 9. These pulses are much stronger than those described above, but, frustratingly, always appeared with center frequency outside the observed frequency span. Figure 9 indicates a probable pulse length of about 1 μs and bandwidth of at least 1.5 MHz. Similar pulses were observed in three other blocks (33, 34, and 35) in this same file, plus two other blocks (26 and 27) in File 42 of this same file set.

Finally, we note that because the threshold for pixel detection was set very high, it is quite likely that many small pulses have been missed. As noted above, these are likely to be detectible using thresholds in the 5σ to 10σ range.

3.3 Bin Detections

As shown above, persistent band-limited signals seem to be the dominant form of RFI in the data analyzed. The most interesting RFI event found from a manual search through a few files is shown in Figures 10 through 14. This is a sequence of blocks from

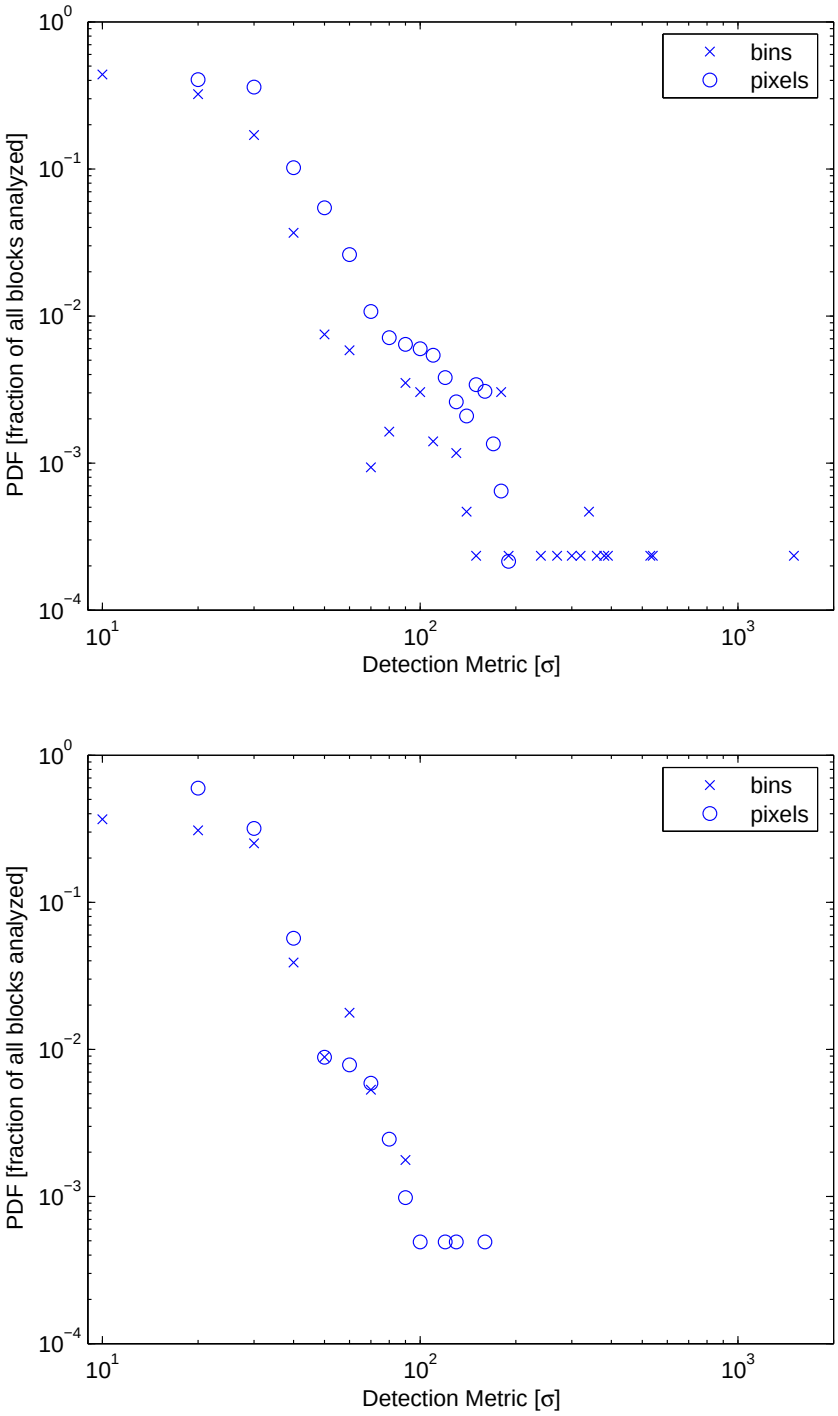

Figure 5: PDFs of pixel and bin event detections in file sets 391 (*top*) and 182 (*bottom*).

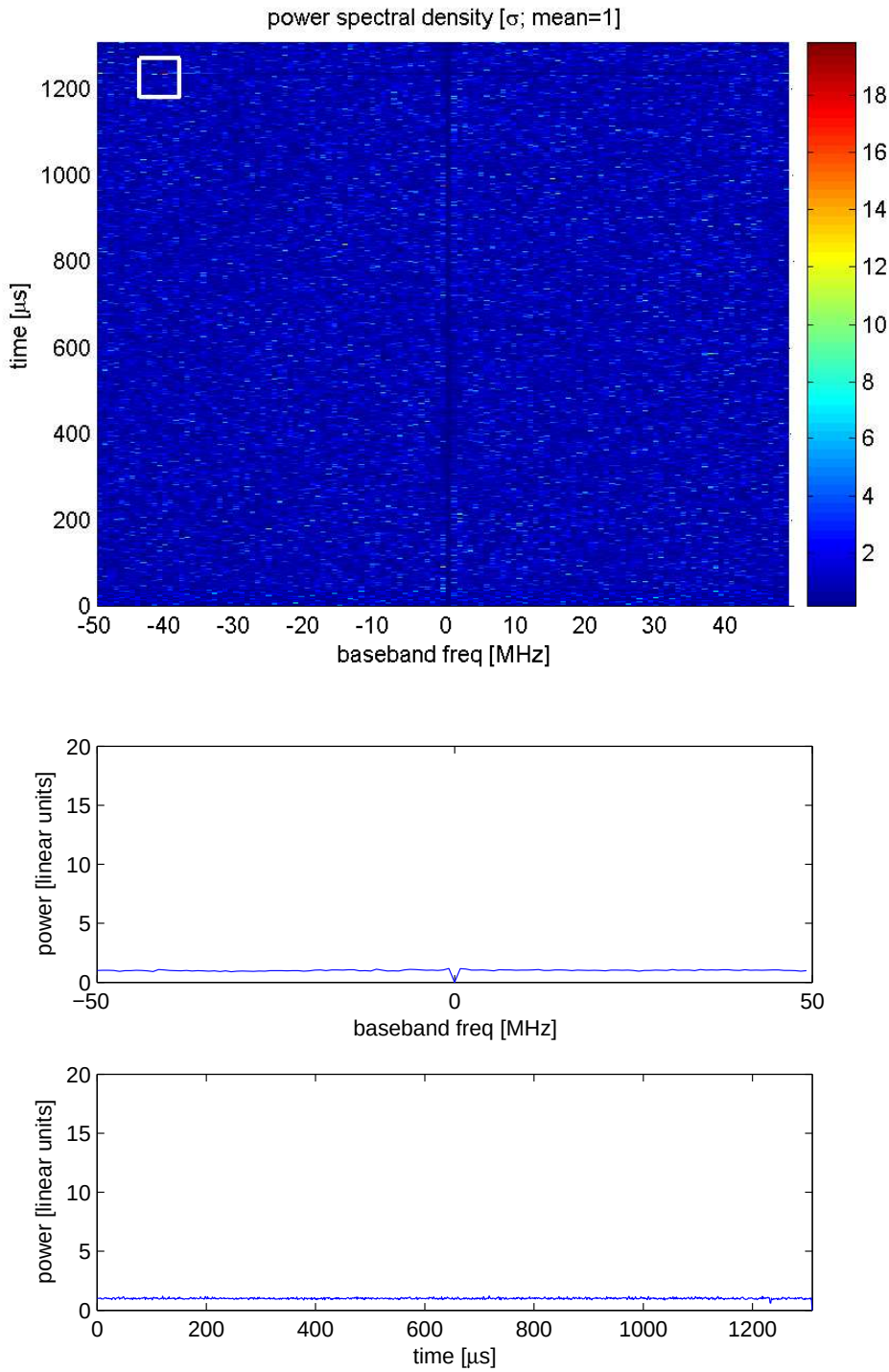

Figure 6: Probable radar pulse detected in file set 391, file 218, block 23. A white square marks the location of the detected pixel in the spectrogram. Despite the fact that the pulse does not appear in the integrated time or frequency auxiliary plots, it triggered a pixel detection with a level of 53.4σ.

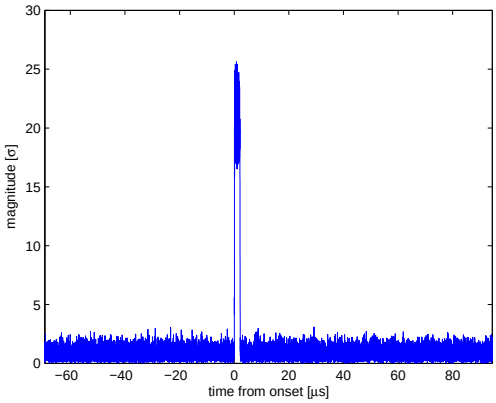

(a) Magnitude vs. time

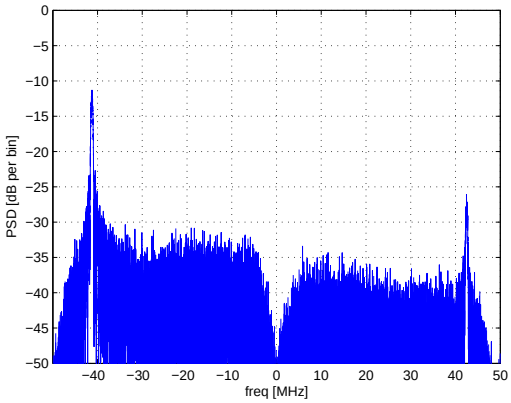

(b) PSD

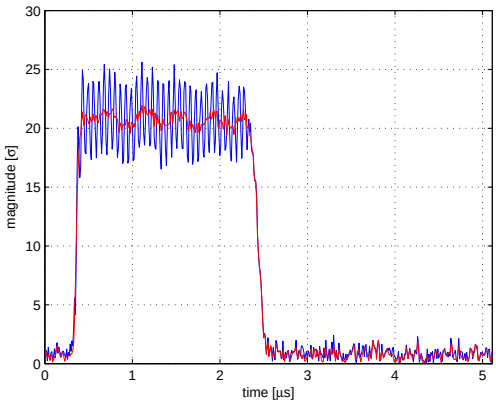

(c) Magnitude vs. time (zoom)
Blue: complete signal.
Red: Upper sideband filtered out

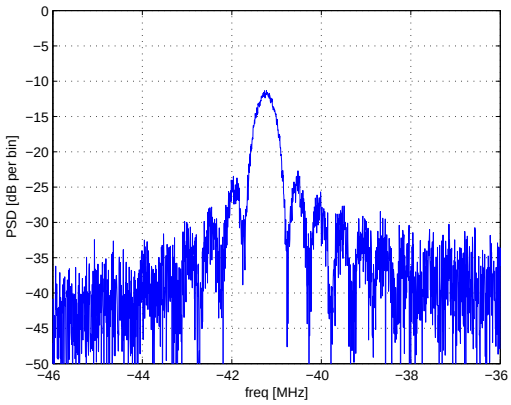

(d) PSD (Zoom)

Figure 7: Follow-up of probable radar pulse detected in Figure 6, using a short segment of raw data around the time of the pulse, and without baseline correction.

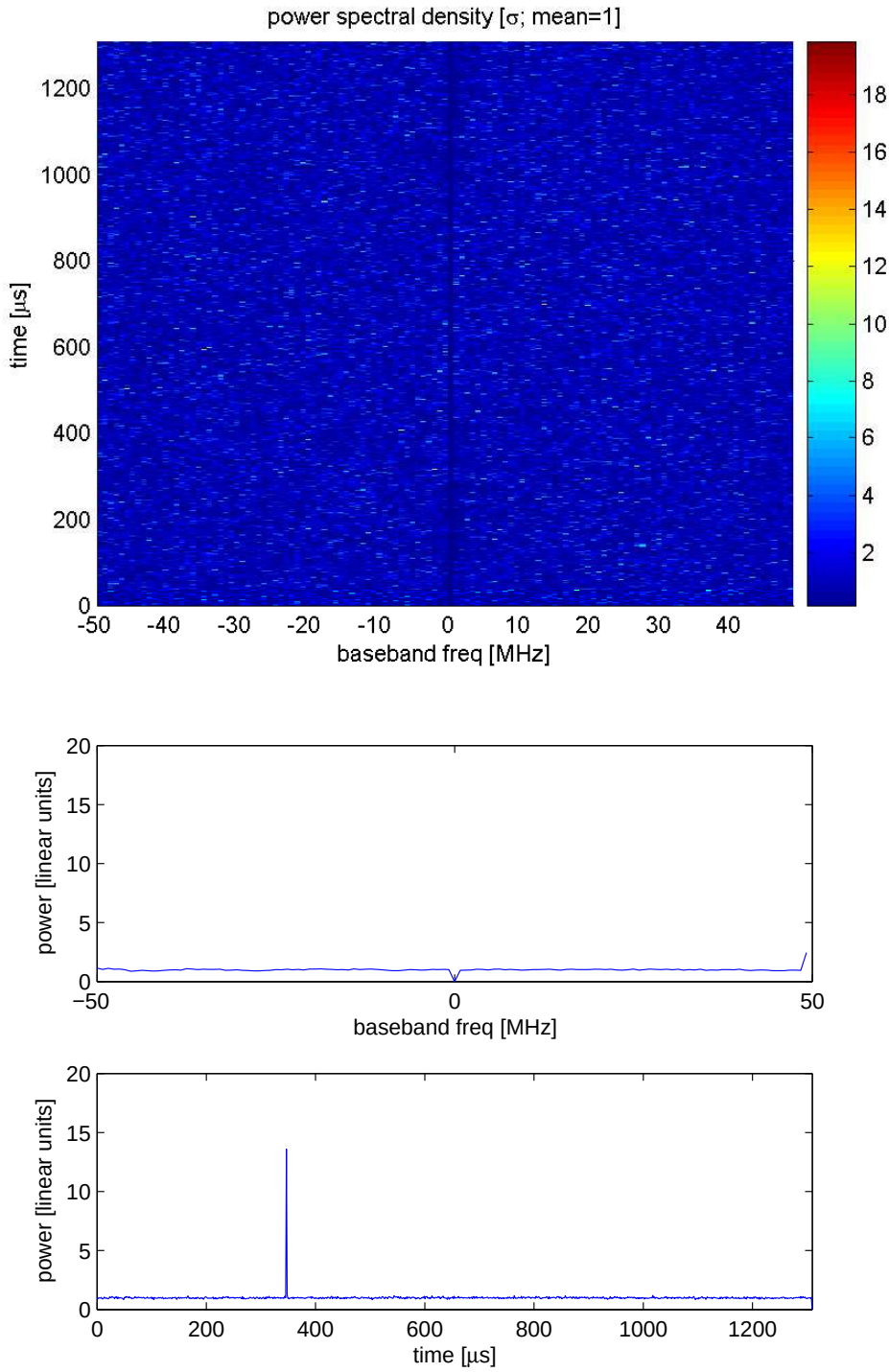

Figure 8: Probable radar pulse detected in file set 391, file 27, block 32. Despite having a center frequency outside the span of the spectrogram, it triggered a pixel detection with a level of 1501σ and is clearly visible in the time series auxiliary plot.

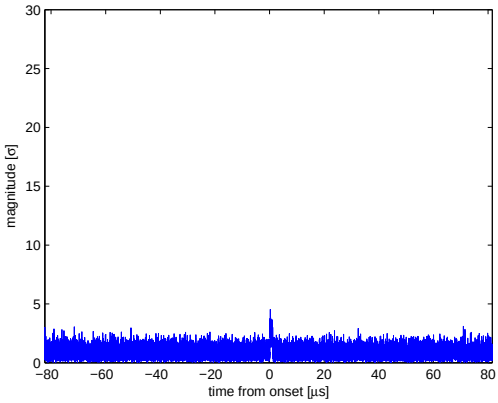

(a) Magnitude vs. time

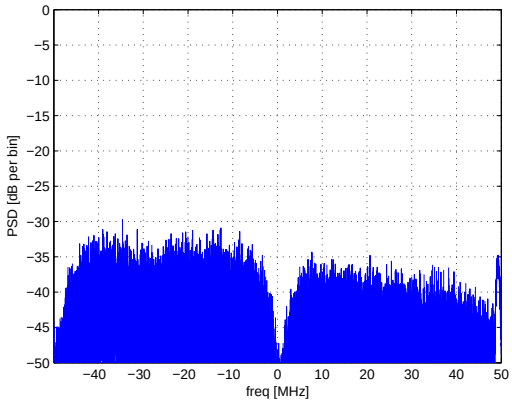

(b) PSD

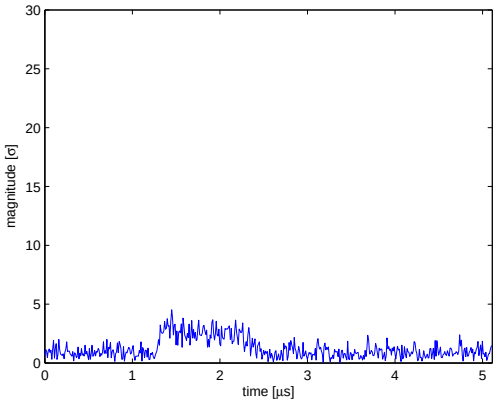

(c) Magnitude vs. time (zoom)

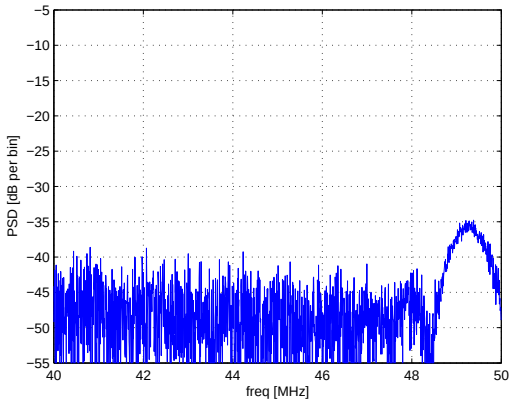

(d) PSD (Zoom)

Figure 9: Follow-up of probable radar pulse detected in file set 391, file 27, block 32 using a short segment of raw data around the time of the pulse, and without baseline correction.

file 290 of file set 391 which show an extremely strong signal which appears to have bandwidth much greater than 100 MHz. Specifically blocks 5, 6, 7, and 8 (Figures 10 through 13) reveal what appear to be only a few sidelobes of a signal which appears have a center frequency far to left. Blocks 10 and 11 exhibited no RFI. Then block 11 exhibited a relatively weak, narrowband signal shown in Figure 14. This exact same behavior was then seen to happen *in reverse* in blocks 30 (corresponding to block 11), 33 (corresponding to block 8), and so on for blocks 34–36.

Figures 15–20 show some other notable events encountered in the manual analysis of a few files. None of these signals have been positively identified as to origin. It should be noted, in fact, that any of these signals, including those shown in the sequence described above, could originate internally; e.g., from some system on the same plane from which the observations were made.

4 Implications for RFI Mitigation Algorithms

The findings of this study are mostly good news in terms of potential for RFI mitigation techniques. Most (93% and 97% for file sets 391 and 182 respectively) of the blocks analyzed exhibited no detectible RFI, suggesting that a perfectly reasonable approach might be simply to discard any block in which RFI is detected. A caveat is that the thresholds for detection in this study were set somewhat high, such that the lack of detections within a block does not necessarily mean there is no RFI in the block; only that the RFI present is unlikely to "significantly" bias a total power measurement of the type traditionally performed in Earth remote sensing.

If the strategy of discarding any block exhibiting RFI is used, it appears that a combination of pixel and bin detection are required to ensure that all significant forms of RFI which are consistently detected. In particular, since much of the RFI observed seems to be persistent (as opposed to pulsed) in nature, and since even strong pulsed RFI may not be strong enough to be reliably detected in total power observations (even with time resolution down to a few microseconds), the "asynchronous pulse blanking" (APB) technique may have limited usefulness. The application of the detection scheme used in APB to data which is channelized to bandwidth on the order of 1 MHz or so, however, is essentially equivalent to pixel detection as performed in this study.

5 Suggested Next Steps

Based on the findings of this study, the following steps should be considered:

1. Despite considerable effort, none of the RFI observed in this study could be conclusively identified as being due to some specific emitter. Indeed, there is no guarantee that any of the RFI identified in this study is truly externally generated, as opposed to having an origin on the same plane or possibly resulting from harmonics or intermodulation created within the instrument. Some more

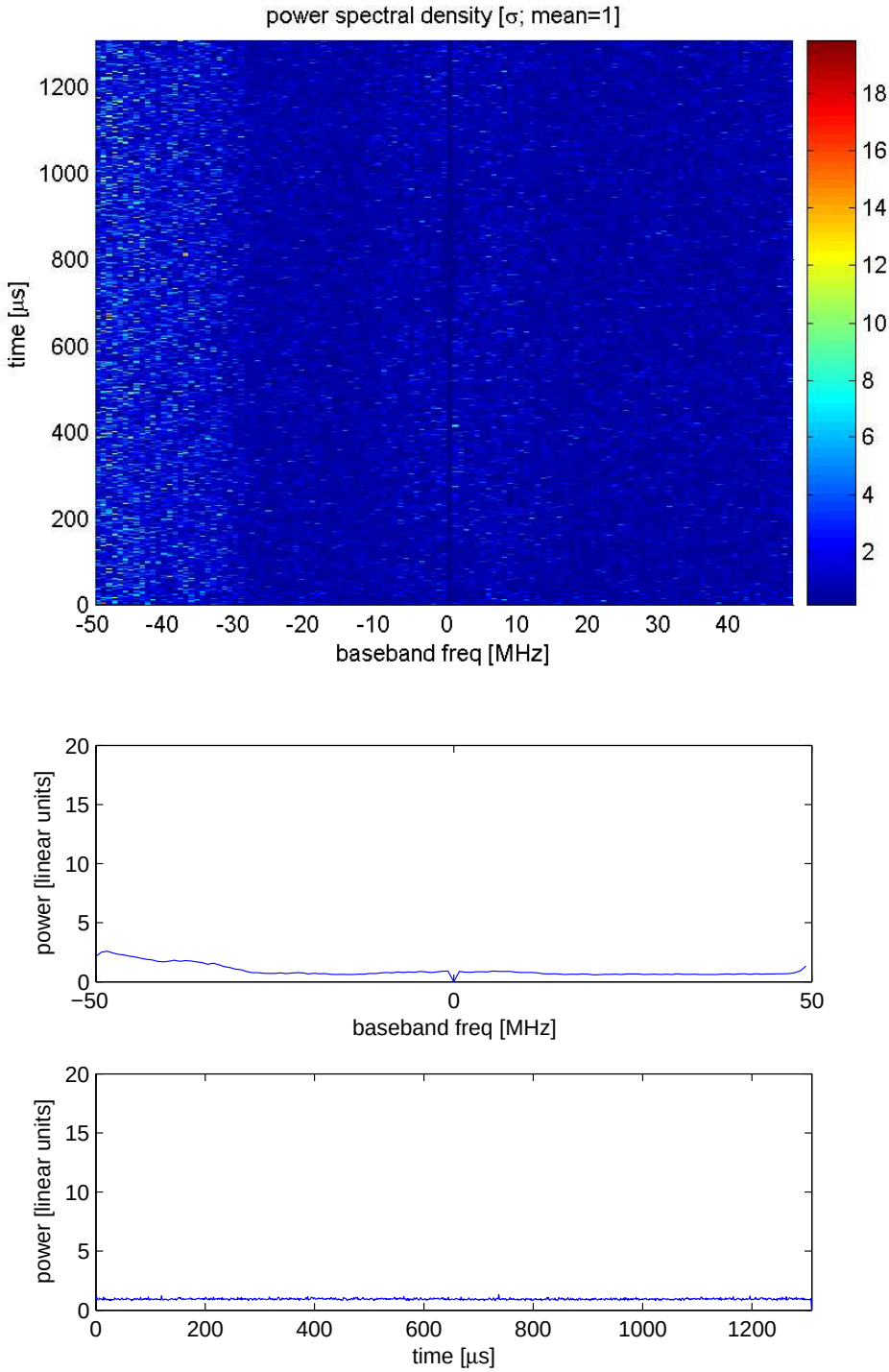

Figure 10: File set 391, file 290, block 5. Block 36 was similar (see text).

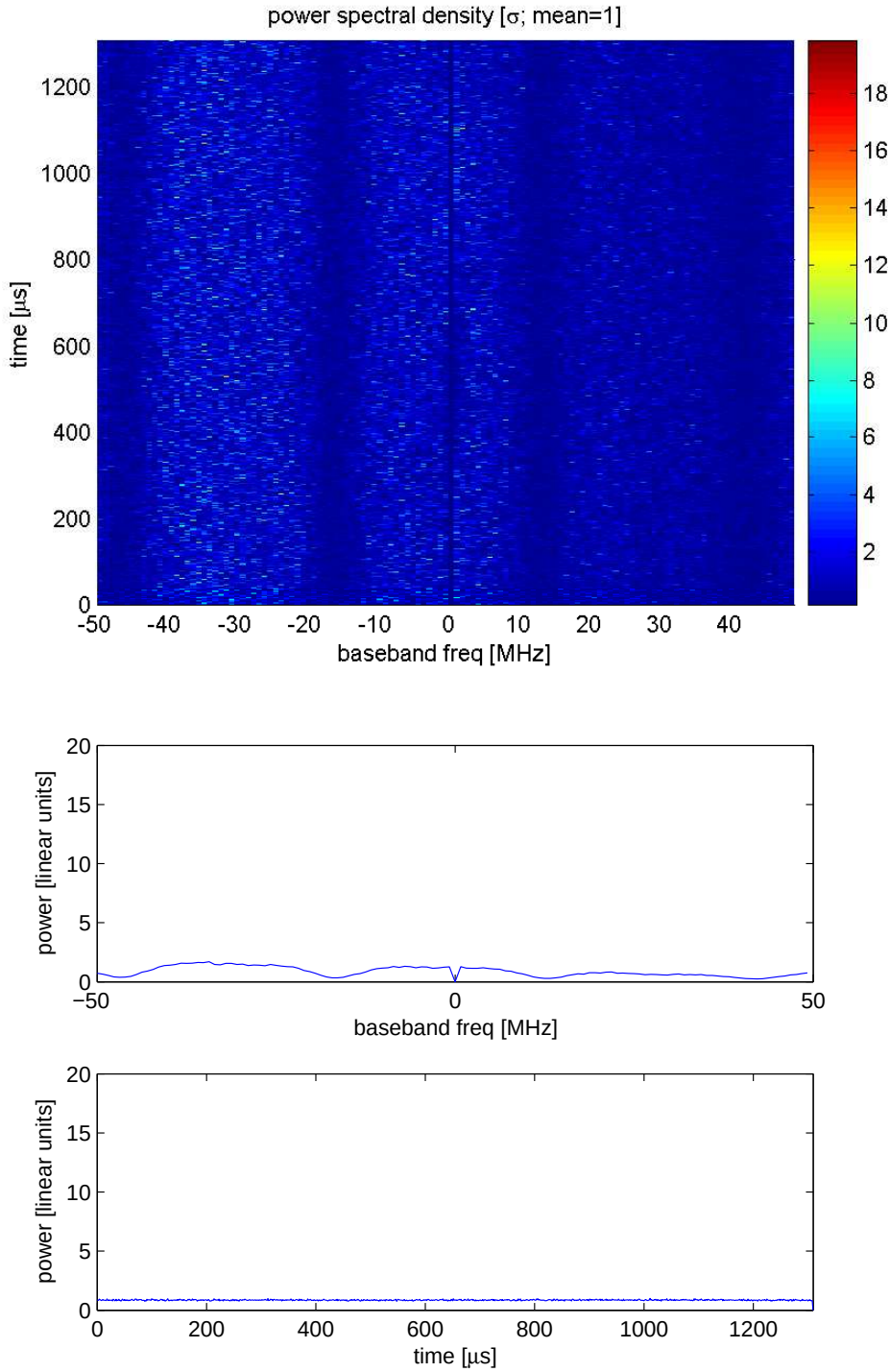

Figure 11: File set 391, file 290, block 6. Block 35 was similar (see text).

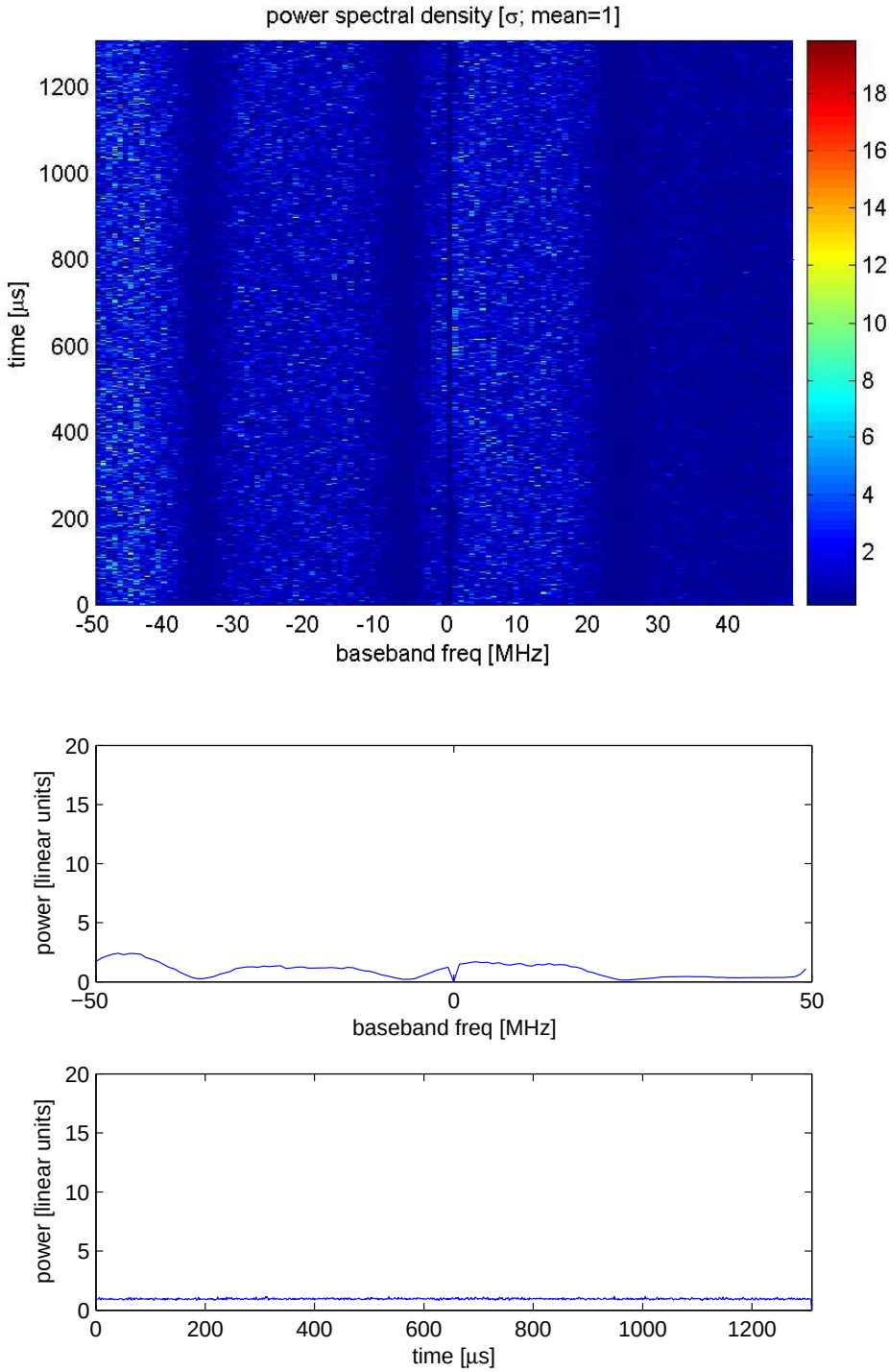

Figure 12: File set 391, file 290, block 7. Block 34 was similar (see text).

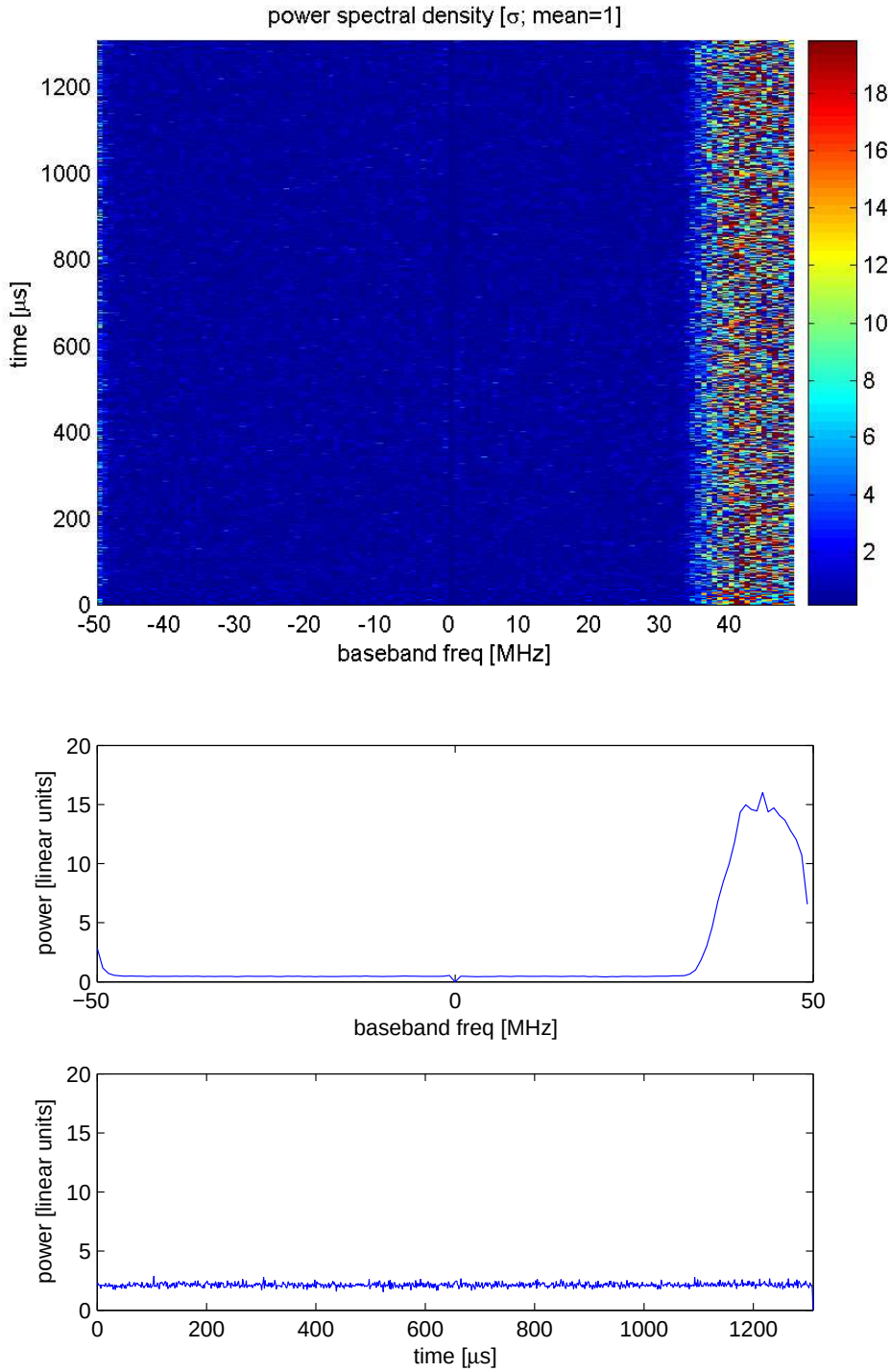

Figure 13: File set 391, file 290, block 8. Block 33 was similar (see text).

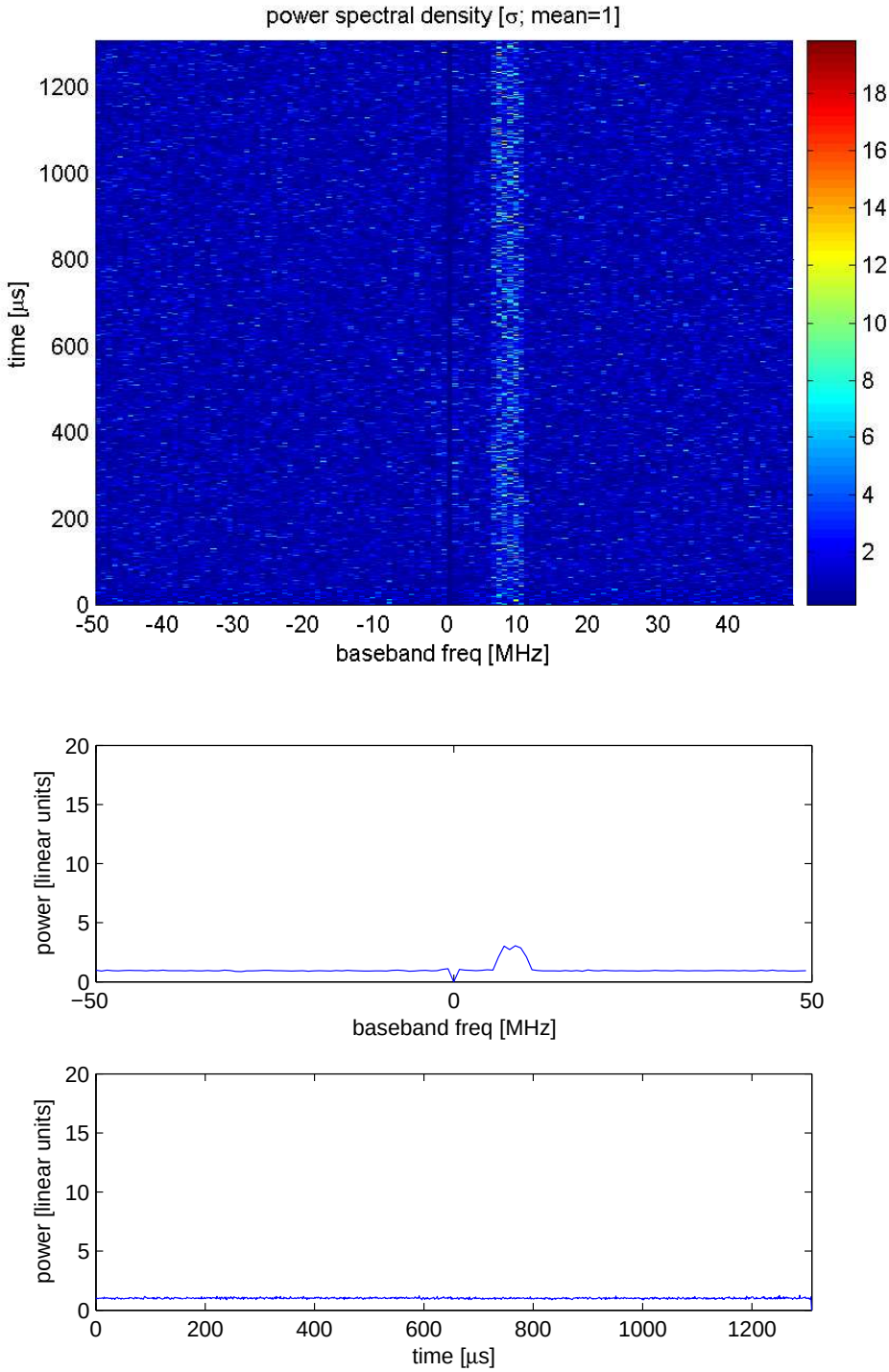

Figure 14: File set 391, file 290, block 11. Block 30 was similar (see text).

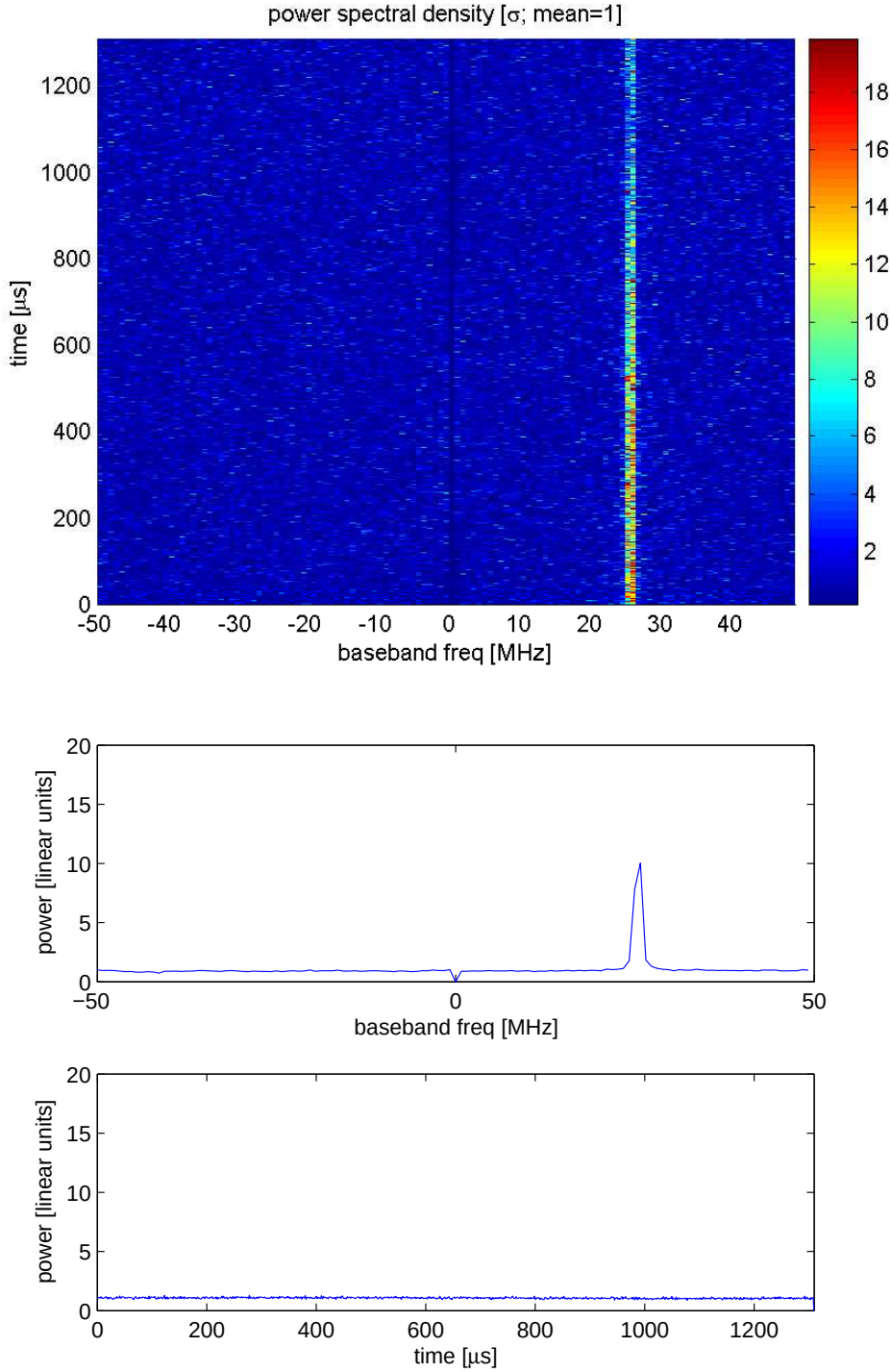

Figure 15: Typical example of a strong narrowband signal. File set 391, file 27, block 7.

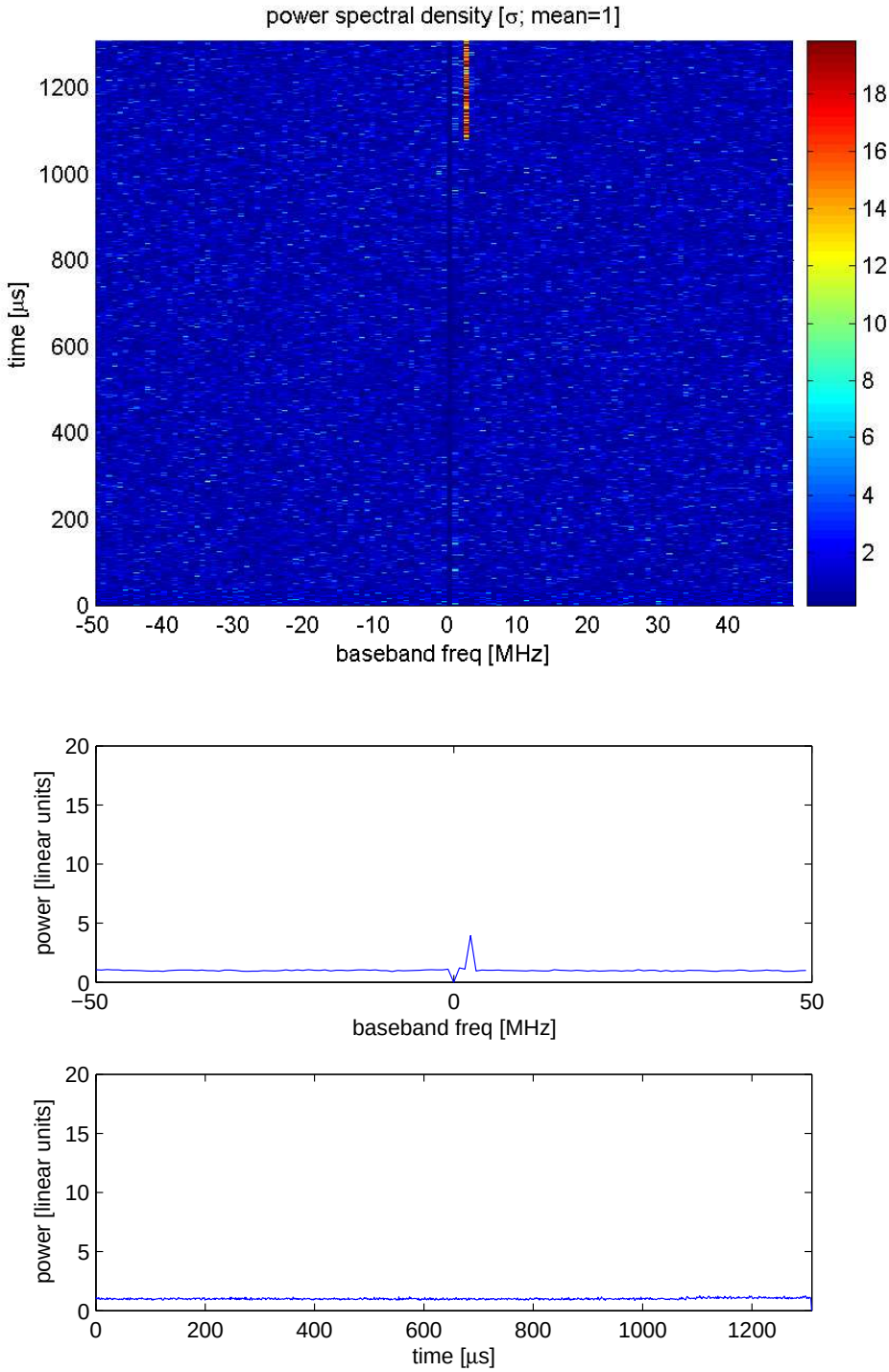

Figure 16: A narrowband signal detected in the process of turning on. File set 391, file 82, block 9.

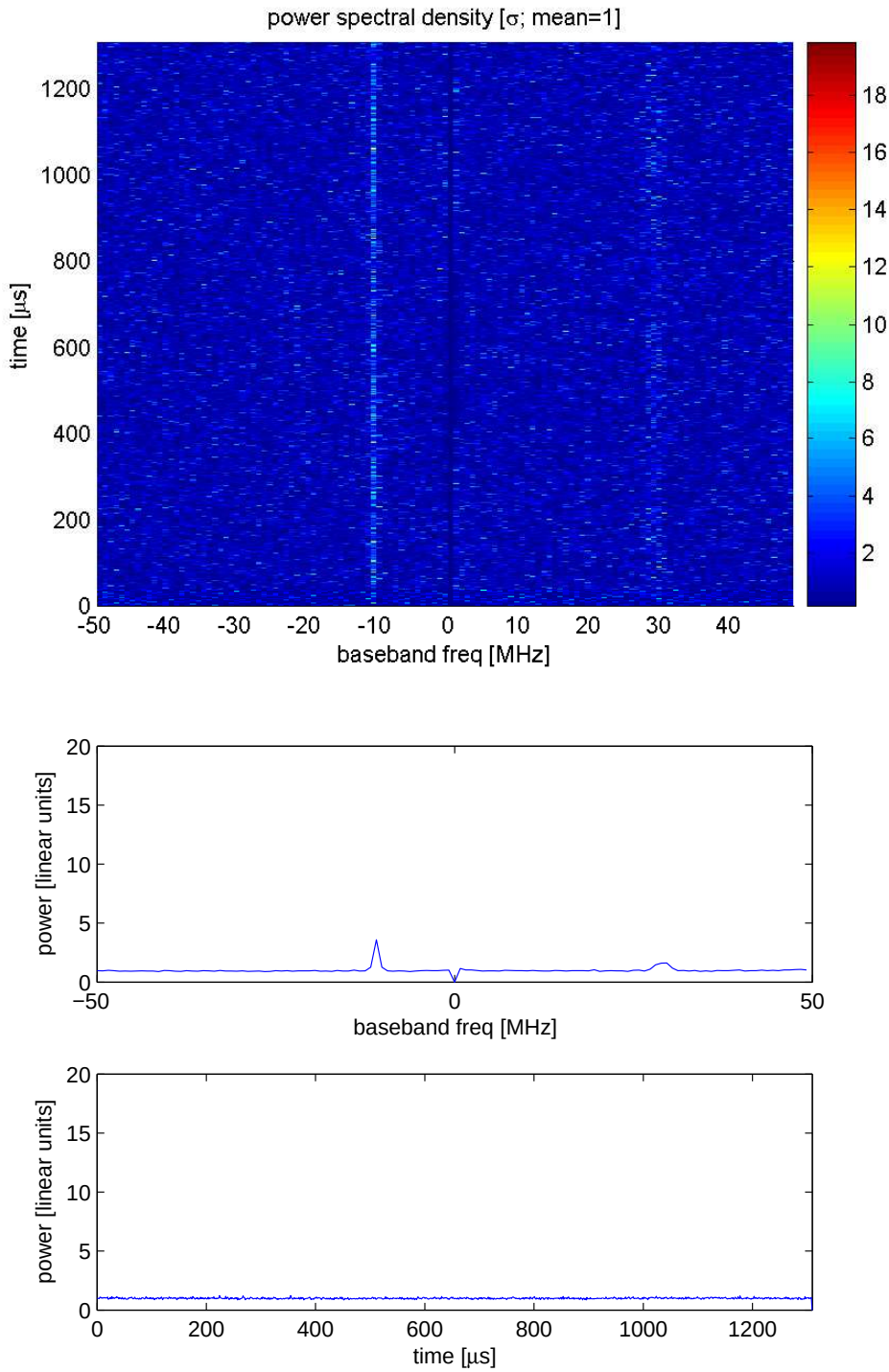

Figure 17: Two narrowband signals. File set 391, file 218, block 10.

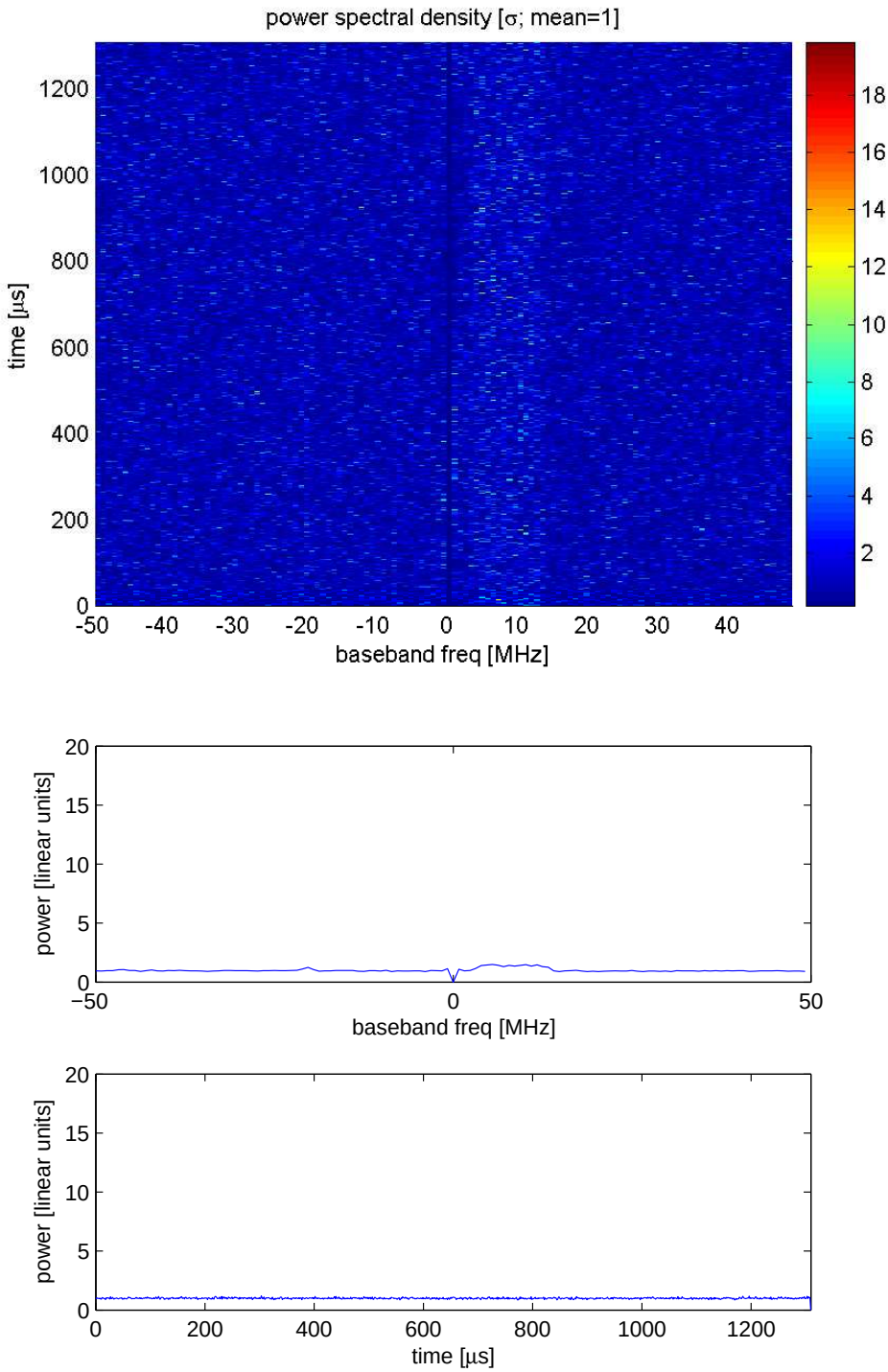

Figure 18: A weak wideband signal. File set 391, file 218, block 12.

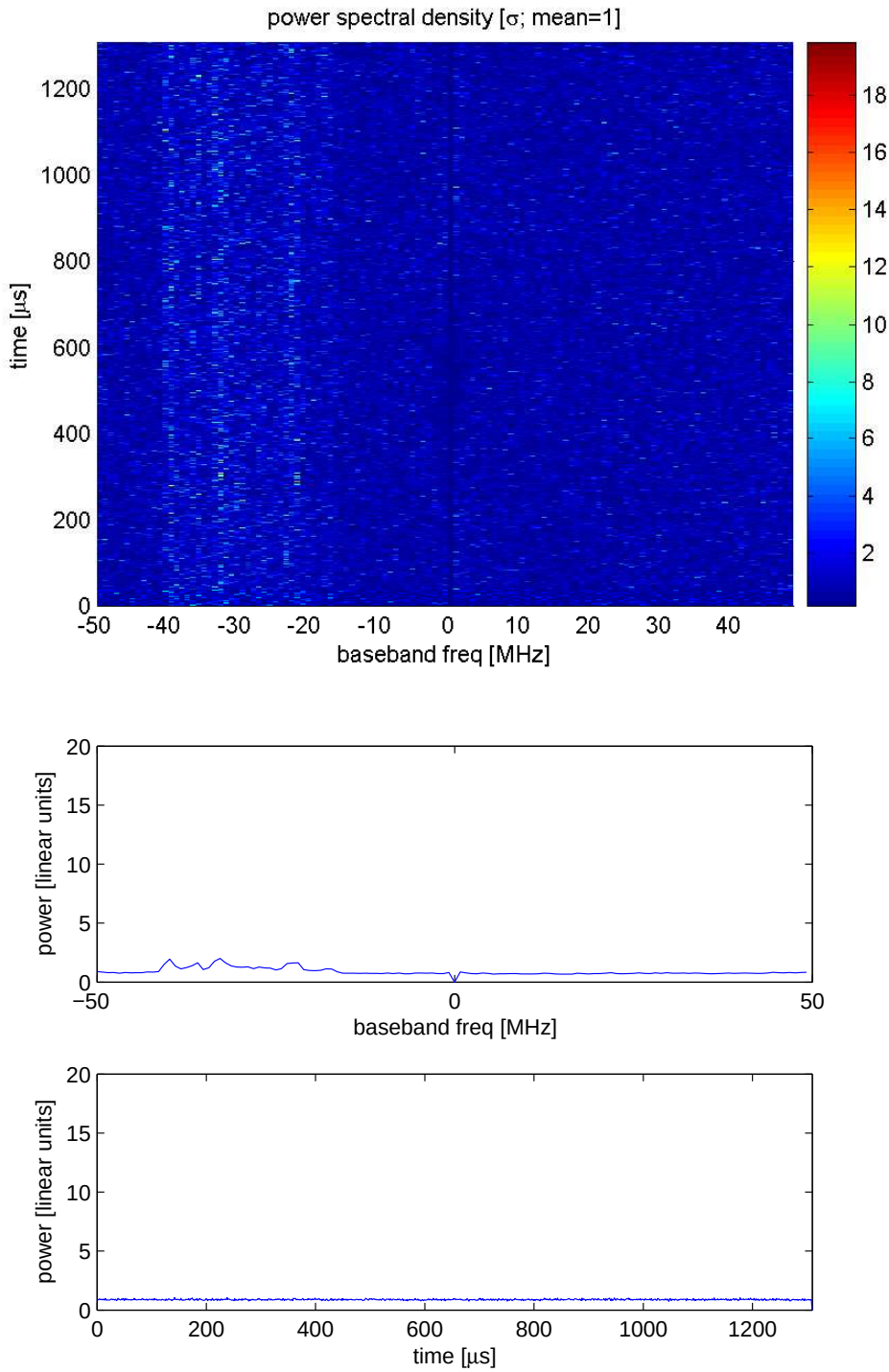

Figure 19: "Claw marks." File set 391, file 42, block 1.

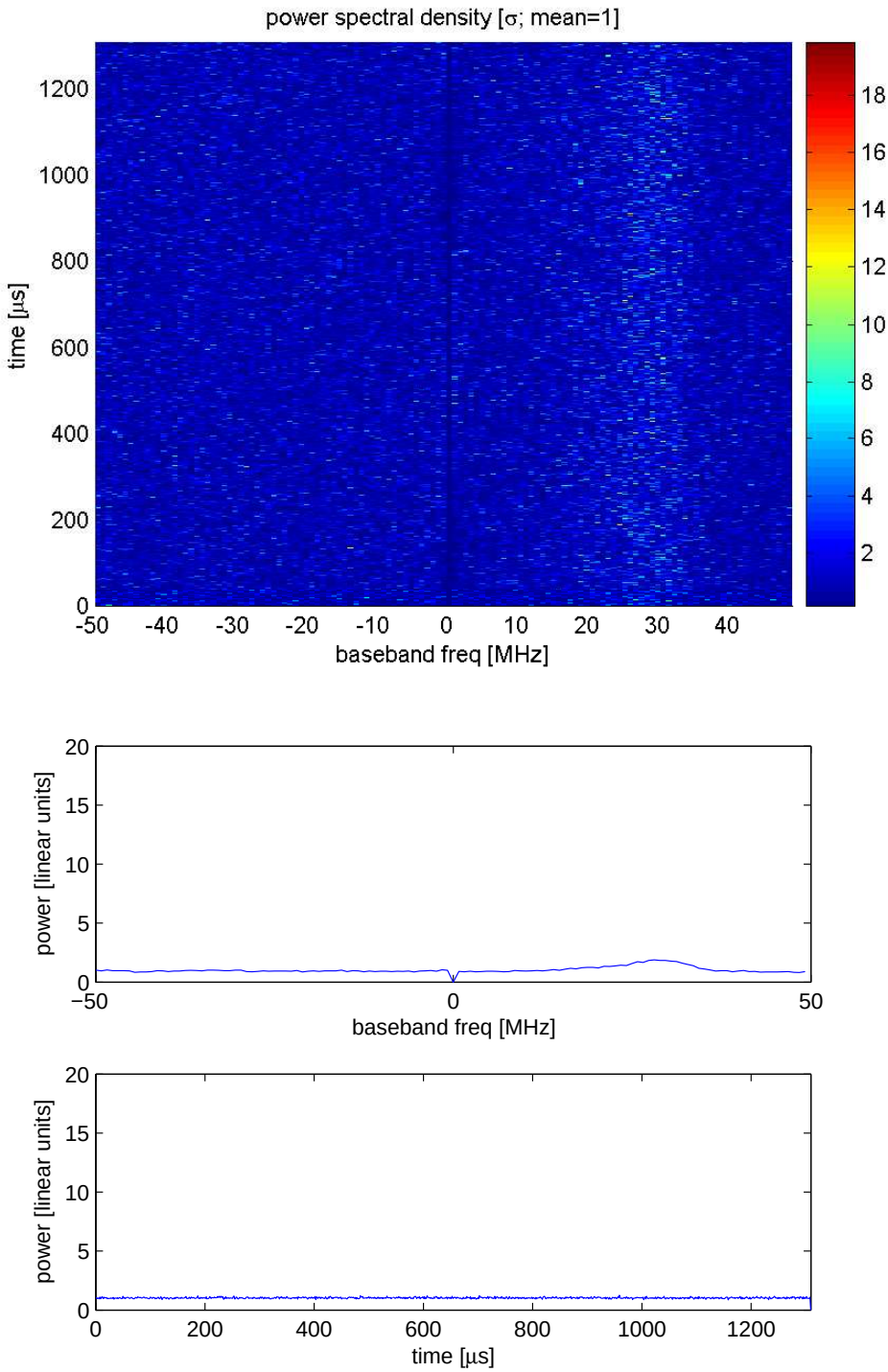

Figure 20: "The heap." File set 391, file 82, block 1.

effort is probably warranted to associate the RFI observed here with known emitters.

2. In this study, there was no attempt to associate RFI events with frequency or antenna pointings. It is likely that at least the former and possibly the latter could yield some additional insight into the source of the RFI. It would also be helpful to determine what fraction (if any) of the 5.5–7.7 GHz span of observation was consistently free of interference; however this may be better done using other observing modes of CISR.

3. Similarly, it may be useful to determine the absolute power density of detected RFI. This will require a careful analysis of the system (including antenna and receiver gains and frequency responses) plus accurate calibration. However, this information would be useful in developing design guidance for future instruments.

4. It is possible some additional insight could be gained by attempting to determine waveform parameters (e.g., symbol rate, modulation scheme, and so on) for signals such as that shown in Figure 13. An initial attempt was made for this particular signal, but proved to be quite difficult due to the uncertainty in carrier frequency and relatively low amount of oversampling due to the large fractional bandwidth of this signal. Progress in this direction will require a three-dimensional search over carrier frequency, symbol timing, and symbol period, which is possible but will require significant additional effort.

5. It would be worthwhile to perform a quick study to determine the performance of the simplest RFI mitigation approach of simply discarding any block with detected RFI. Anticipating the challenges of practical implementation, it might also be worthwhile to investigate how crude (simple) the algorithm could be and still be effective.

6. There may be some value in extending the manual search over all files captured (only 6 files were searched manually in this study), since additional forms of "interesting" RFI may be revealed.

References

[1] J. T. Johnson *et al.*, "Airborne radio frequency interference studies at C-band using a digital receiver," *Proc. IEEE Geo. and Remote Sensing Sym.*, Anchorage, AK, Sep 2004.

[2] S.W. Ellingson and G.A. Hampson, "Mitigation of Radar Interference in L-Band Radio Astronomy," *Astrophysical J. Supp. Ser.*, Vol. 147, No. 1, pp. 167–176, July 2003.